Vibrationally resolved photoelectron spectroscopy of silicon cluster anions Si_n^- $(n=3-7)$

Cangshan Xu,[a] Travis R. Taylor, Gordon R. Burton,[b] and Daniel M. Neumark
Department of Chemistry, University of California, Berkeley, California 94720 and Chemical Sciences Division, Lawrence Berkeley Laboratory, Berkeley, California 94720

(Received 28 July 1997; accepted 10 October 1997)

Photoelectron spectra of Si_n^- $(n=3-7)$ have been measured at several photodetachment energies. The anions were created using a pulsed discharge source, resulting in considerably colder clusters than in earlier work. As a result, vibrationally resolved spectra were obtained for larger clusters and more electronic states than in previous studies of these species, leading to more accurate electron affinities, term energies, and vibrational frequencies for the ground and excited electronic states of the neutral clusters. The assignments of excited states were aided by *ab initio* calculations and photoelectron angular distributions. © *1998 American Institute of Physics.* [S0021-9606(98)02703-2]

I. INTRODUCTION

Small silicon clusters have been the subject of a series of experimental and theoretical studies during the last ten years. This work has been in part motivated by the important role that silicon plays in the electronics industry, since studies of silicon clusters can provide insight into how the optical and electronic properties of semiconductors evolve from the molecular to macroscopic size regimes. Silicon clusters are also of considerable interest from the perspective of fundamental chemistry. Silicon lies directly below carbon in the periodic table, but *ab initio* calculations predict that the structures of silicon clusters differ substantially from carbon clusters in the same size range. While small carbon clusters form linear chains and rings, silicon clusters are predicted to form more compact three-dimensional structures. This difference is attributed to the much weaker π-bonding in Si clusters, thereby favoring structures with more single bonds. Thus, for example, the ground state of C_5 is linear, whereas calculations indicate the ground state of Si_5 to be a trigonal bipyramid. The remarkable differences between the structures for silicon and carbon clusters have motivated the experiments described in this paper, in which anion photoelectron spectroscopy is used to probe the vibrational frequencies and low-lying electronic states of Si_n $(n=3-7)$ clusters.

The experimental investigation of silicon clusters in this size range has proved to be a challenge, but there has been considerable progress in recent years. Cheshnovsky *et al.* measured anion photoelectron spectra of Si_n^- $(n\leqslant 13)$ clusters, yielding electron affinities and a qualitative picture of the electronic states of the neutral clusters.[1] The experimental resolution was insufficient to observe any vibrational structure, and no assignments of the electronic states were attempted. Neumark and co-workers later obtained vibrationally resolved anion photoelectron spectra[2] and zero electron kinetic energy (ZEKE) spectra of Si_3^- and Si_4^-.[3,4] These spectra showed well-resolved vibrational progressions for several electronic bands, yielding vibrational frequencies and electronic term values for some of the low-lying electronic states of Si_3 and Si_4. Eberhardt and co-workers have recently measured the photoelectron spectrum of Si_7^- with sufficient resolution to observe a vibrational progression.[5] These gas phase studies have been complemented by matrix isolation spectroscopy. Jarrold and co-workers have measured Raman spectra of mass-selected clusters in matrices, yielding some vibrational frequencies for the ground electronic states of silicon clusters up to Si_7 (excluding Si_5).[6] Infrared spectra of silicon clusters in matrices were also obtained recently and assigned to Si_3, Si_4, Si_6, and Si_7 by Li *et al.*[7]

Ab initio calculations of the properties of silicon clusters have been carried out by several investigators.[8–22] These calculations have proved invaluable in understanding the various experiments carried out on Si clusters. For example, the geometries and vibrational frequencies of neutral silicon clusters up to Si_{10} were calculated by Raghavachari[9] before any of the above experiments were carried out. This was followed by calculations by Raghavachari and Rohlfing on the negative ion geometries and frequencies as well as the low-lying excited states for several of the neutral clusters,[15–17] work which greatly aided in interpreting the photodetachment spectra of Si_3^- and Si_4^-.

This paper represents an extension of our earlier work on the photoelectron spectroscopy of silicon cluster anions.[2] Our original attempts to measure vibrationally resolved photoelectron spectra of clusters larger than Si_4^- were unsuccessful. The laser ablation source originally used to produce the anions has been replaced by a new method which produces substantially colder ions, resulting in less spectral congestion from ''hot bands.'' As a result, we have obtained improved spectra for Si_3^- and Si_4^-, as well as vibrationally resolved spectra of $Si_5^- - Si_7^-$. The new spectra for Si_3^- and Si_4^- provide more accurate electron affinities and vibrational frequencies, along with a clearer picture of the low-lying electronic states of the neutral clusters. The spectra of the three larger clusters

[a]Current address: Lam Research Corporation, 77 West Montague Expressway, Milpitas, CA 95035.
[b]Current address: Whiteshell Laboratories, Pinawa, Manitoba, ROE 1L0, Canada.

provide new information on the anion and neutral geometries as well as the excited state energies of the neutral clusters.

II. EXPERIMENT

The experiments were carried out on a time-of-flight negative ion photoelectron spectrometer. The instrument has been described in detail previously,[23] recent modifications have resulted in considerably improved mass resolution.[24] Silicon cluster anions are generated by expanding a dilute mixture of SiH_4 (5% SiH_4, 95% He) through a pulsed piezoelectric valve/pulsed electrical discharge source.[25] In this source, the gas pulse from the beam valve passes through two stainless steel plates between which a high voltage (about 600 V) pulse is applied. The pulse then expands into a vacuum chamber. The resulting free jet is collimated by a 2 mm diam skimmer located 1.5 cm downstream from the ion source and then enters a differentially pumped region. Here, the ions are extracted from the beam and enter a time-of-flight mass spectrometer with a linear reflectron stage. The accelerated ions separate in time and space according to their mass-to-charge ratios, and are selectively detached by a pulsed Nd:YAG laser.

Four different wavelengths, the third and fourth harmonics (355 nm, 3.493 eV and 266 nm, 4.657 eV, respectively) from a pulsed Nd:YAG laser and the first Stokes Raman lines (416 nm, 2.977 eV and 299 nm, 4.141 eV) of these wavelengths generated in a high-pressure H_2 cell are used in these experiments. The photoelectron kinetic energy is measured by time-of-flight in a field-free flight tube 100 cm in length. The instrumental resolution is 8–10 me V for an electron kinetic energy (eKE) of 0.65 eV and degrades as $(eKE)^{3/2}$. The polarization angle θ between the laser polarization and the direction of electron collection can be varied using a polarization compensator (New Focus, model 5540). The variation of peak intensities with θ is used to separate the contributions of different electronic states to the photoelectron spectra. Secondary electrons resulting from scattered photons necessitated background subtraction in the 266 nm spectra.

III. RESULTS

Figure 1 shows the anion mass spectrum obtained from the discharge source. Bare silicon clusters as well as partially hydrogenated species $Si_xH_y^-$ are observed. Figure 2 compares the photoelectron spectra of Si_4^- at a photodetachment wavelength of 355 nm (3.493 eV) using the pulsed discharge and laser ablation ion sources. It is clear upon inspection that the former spectrum shows considerably better-resolved vibrational structure, which we attribute to a lower vibrational temperature and therefore less spectral congestion from ''hot band'' transitions originating from vibrationally excited anions.

The photoelectron spectra for $Si_3^- - Si_7^-$ at a variety of wavelengths are presented in Figs. 3–8. Spectra were taken at laser polarization angles of 90°, 54.7° (magic angle), and 0° for each anion. The spectra consist of bands corresponding to transitions from the anion to various neutral electronic states. Vibrational structure is resolved in many of these bands. For each peak, the electron kinetic energy (eKE) is given by:

$$\mathrm{eKE}=h\nu-\mathrm{EA}-T_0^{(0)}+T_0^{(-)}-E_v^{(0)}+E_v^{(-)}, \tag{1}$$

where $h\nu$ is the laser photon energy, EA is the adiabatic electron affinity of the neutral species, $T_0^{(0)}$ and $T_0^{(-)}$ are the term values of the neutral and anion electronic states, and $E_v^{(0)}$ and $E_v^{(-)}$ are the neutral and anion vibrational energies, respectively, above the zero point energy. The photoelectron angular distribution is given by[26]

$$\frac{d\sigma}{d\Omega}=\frac{\sigma_{\mathrm{total}}}{4\pi}\left[1+\beta(E)P_2(\cos\,\theta)\right], \tag{2}$$

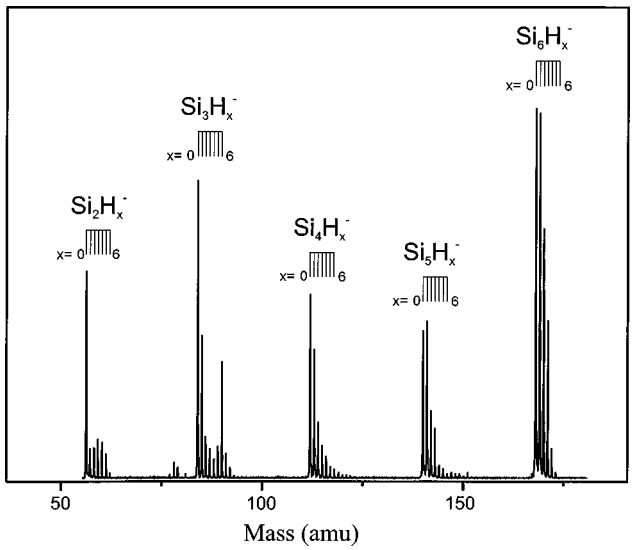

FIG. 1. Mass spectrum of bare silicon anion clusters and corresponding silicon hydride anions generated from the discharge ion source.

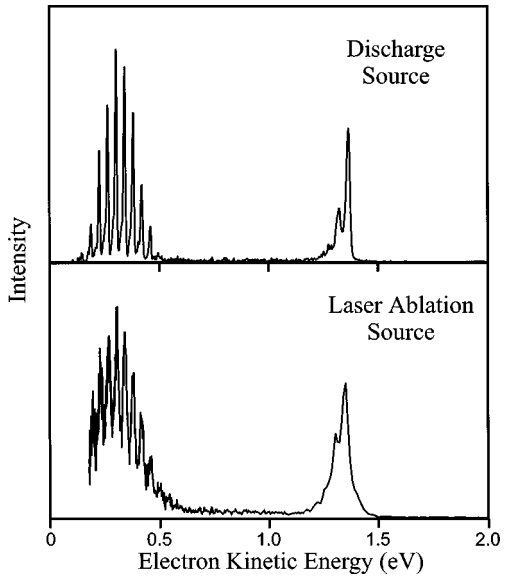

FIG. 2. Si_4^- photoelectron spectra at 355 nm using different ion sources. The discharge source generates substantially colder ions than the traditional laser ablation source.

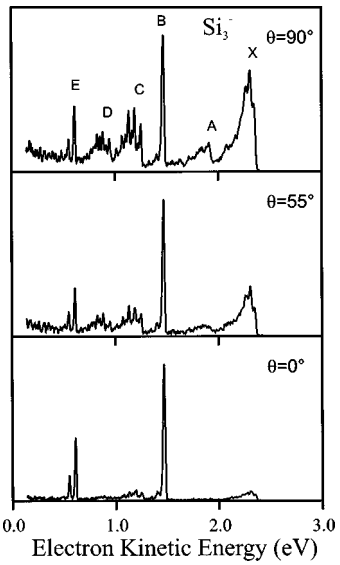

FIG. 3. Photoelectron spectra of Si_3^- taken at 266 nm. Laser polarization angles are θ=90°, 55°, and 0° with respect to direction of electron collection.

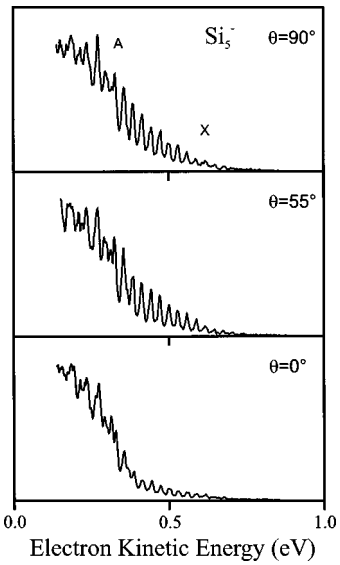

FIG. 5. Photoelectron spectra of Si_5^- taken at 355 nm. Laser polarization angles are θ=90°, 55°, and 0° with respect to direction of electron collection.

where σ_{total} is the total photodetachment cross section and $\beta(E)$ is the asymmetry parameter, varying from -1 to 2. One can determine β for each peak in the photoelectron spectrum through its intensity variation with laser polarization angle. The β parameter for each electronic band is then determined by averaging values of the constituent peaks.

The Si_3^- spectrum at 266 nm, Fig. 3, shows six distinct bands labeled X, and $A-E$. Bands X and A at high electron energy are essentially the same as in our previous spectrum at this wavelength,[2] with each showing some vibrational structure superimposed on a broad background. Band B consists of a very short progression, dominated by the most intense peak of the spectrum at eKE=1.463 eV. The peak spacing of band B is 500 ± 20 cm^{-1}. The band that was labeled as band C in our earlier study is better resolved here and clearly consists of two bands, labeled as bands C and D in Fig. 3. Both show regular progressions. Band C consists of five main peaks with an average spacing of 480 ±20 cm^{-1}. There is a set of less intense peaks with the same peak spacing shifted 260 cm^{-1} towards lower eKE from the main progression. A similar pattern is observed in band D. The intensity profile of band E resembles that of band B, with a single intense peak and a rapid drop of intensity towards lower eKE. The peak spacing in band E is 480 ±20 cm^{-1}. Bands B and E have β parameters of 1.9 and 1.5, respectively, both showing high intensity at θ=0°. These values are considerably larger than those for bands X, A, C, and D, for which $\beta=-0.2$, -0.5, 0.2, and 0, respectively.

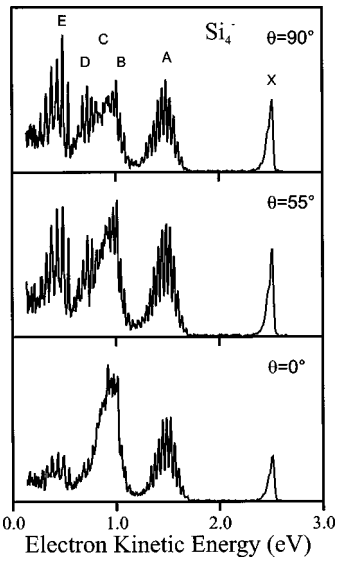

FIG. 4. Photoelectron spectra of Si_4^- taken at 266 nm. Laser polarization angles are θ=90°, 55°, and 0° with respect to direction of electron collection.

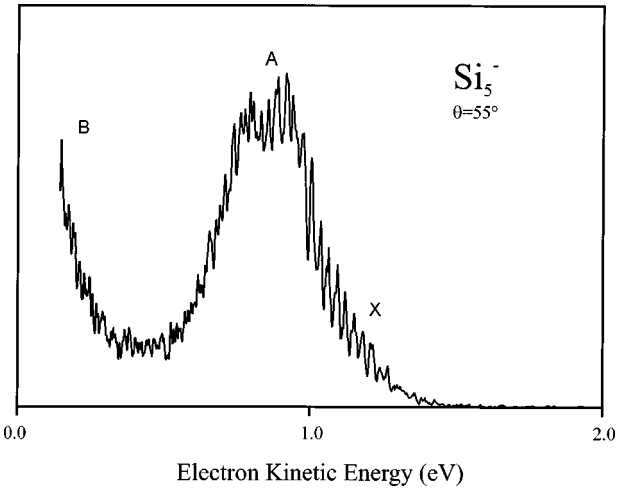

FIG. 6. Photoelectron spectra of Si_5^- taken at 299 nm. Laser polarization angle is θ=55° (magic angle) with respect to direction of electron collection.

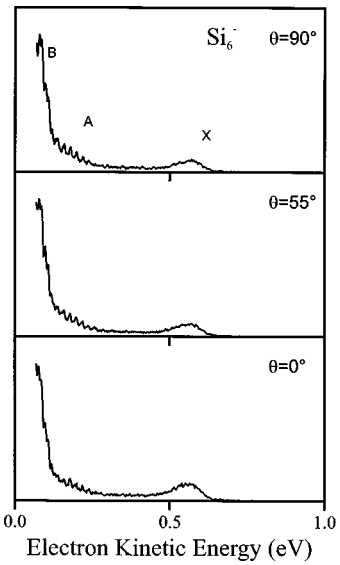

FIG. 7. Photoelectron spectra of Si_6^- taken at 355 nm. Laser polarization angles are $\theta=90°$, 55°, and 0° with respect to direction of electron collection.

The Si_4^- photoelectron spectra at 266 nm in Fig. 4 are substantially improved over our previous spectra at this wavelength.[2] The vibrational progression of $310\pm20\ cm^{-1}$ comprising band *A* is now clearly resolved, and in fact resembles our earlier photoelectron spectrum at 355 nm (Fig. 2) where the energy resolution is higher because the electrons are slower. At lower electron kinetic energies, we now observe three distinct bands labeled *B*, *C*, and *D*, which appeared in our earlier spectrum to be a single structured band (previously labeled band *B*). Bands *B* and *D* show regularly spaced vibrational transitions, while band *C* does not. At low eKE, band *B* is not resolved due to overlap with band *C*. Seven peaks spaced by $290\pm20\ cm^{-1}$ are apparent in band *B* starting at eKE=1.160 eV; the peak spacing and intensity profile are similar to the first several peaks of band

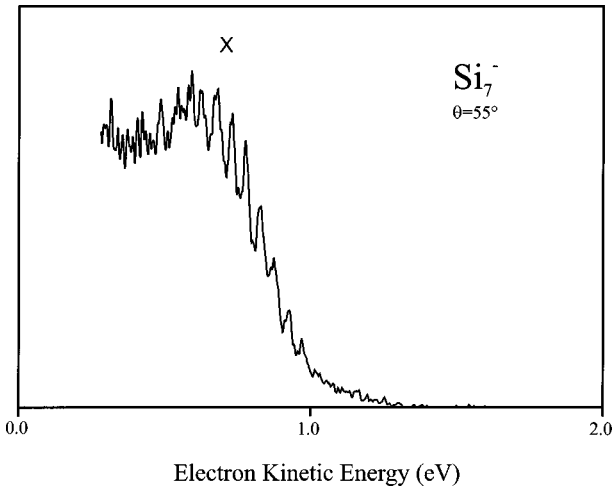

FIG. 8. Photoelectron spectrum of Si_7^- taken at 416 nm. Laser polarization angle is $\theta=55°$ (magic angle) with respect to direction of electron collection.

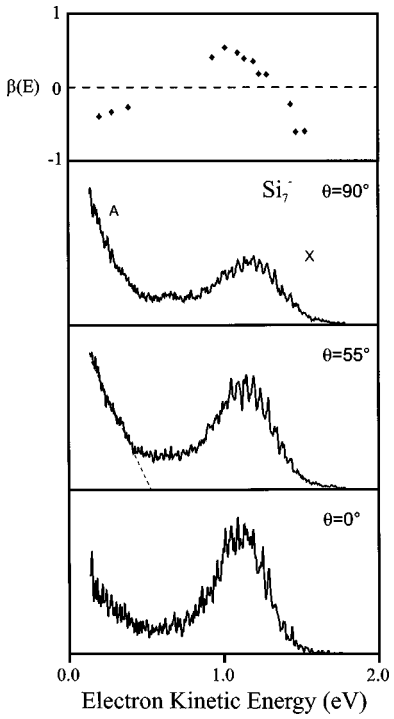

FIG. 9. Photoelectron spectra of Si_7^- taken at 355 nm. Laser polarization angles are $\theta=90°$, 55°, and 0° with respect to direction of electron collection. Top panel shows $\beta(E)$ parameters.

A. Band *D*, on the other hand, consists of six peaks with an average spacing of $355\pm20\ cm^{-1}$. Band *E* shows a well-resolved progression of six peaks spaced by $450\pm20\ cm^{-1}$. The polarization studies indicate band *C* is the most intense band at $\theta=0°$ with $\beta=0.8$, whereas band *E* is the largest band at $\theta=90°$ with $\beta=-0.1$. For bands *X*, *A*, *B*, and *D*, $\beta=0.2$, 0.5, 0.3, and 0, respectively.

The polarization dependence of the spectra of Si_5^- at 355 nm (Fig. 5) clearly shows that two electronic bands, labeled *X* and *A*, contribute to the spectra. Band *X* consists of a regular, well-resolved progression of at least 15 peaks with an average spacing of $233\pm20\ cm^{-1}$. The apparent origin of this transition is at 0.735 eV, although this is very approximate due to the extended nature of the progression. Band *A* is most apparent at $\theta=0°$. It corresponds to the transition to a low-lying excited state of Si_5. While band *A* is structured, it does not show a regular progression as was seen in band *X*. Only part of band *A* is seen at 355 nm. The photoelectron spectrum of Si_5^- was also measured at a higher detachment energy of 4.141 eV (299 nm), shown in Fig. 6. Band *A* can be seen here in its entirety, although there is still no obvious pattern to the vibrational structure.

The photoelectron spectra of Si_6^- at 355 nm, shown in Fig. 7, is comprised of three bands labeled *X*, *A*, and *B*. Band *X* is a weak unstructured transition that reaches a maximum at eKE=1.13 eV; its apparent onset occurs at eKE =1.28 eV. Attempts to observe vibrational structure in band *X* by measuring its photoelectron spectrum at 416 nm were unsuccessful. Band *A*, representing a transition to an excited state of Si_6, consists of seven resolved peaks starting at eKE

TABLE I. QCISD(T)/6-31G* optimized geometries, frequencies, and normal coordinate displacements for Si_3.[a]

	States	QCISD(T)/6-311+G(3DF) energy (Hartrees)	T_e(eV)	R(1-2)(Å)	R(1-3)(Å)	Angle(1-2-3)	Frequencies (cm^{-1})/ΔQ(Å $amu^{1/2}$)
Si_3^-	$^2A_1(C_{2v})$	−867.125 32	−2.21	2.261	2.437	65.2°	297(a_1), 370(b_2), 533(a_1)
Si_3	$^1A_1(C_{2v})$	−867.043 93	0.0	2.191	2.806	79.6°	148(a_1), 525(b_2), 551(a_1)
	$^3A_2'(D_{3h})$	−867.043 30	0.02	2.290	2.290	60.0°	285(e), 522(a_1)
	$^3A_1(C_{2v})$	−867.010 28	0.92	2.281	2.436	64.6°	325(a_1)/0.05, 405(b_2), 523(a_1)/0.09
	$^3B_1(C_{2v})$	−867.002 87	1.12	2.333	2.579	67.1°	247(a_1)/0.38, 321(b_2), 481(a_1)/0.41

[a]Geometries, frequencies, and energies from Ref. 17.

TABLE II. MP2/6-31G* optimized geometries, frequencies, and normal coordinate displacements for Si_4.[a]

	States	QCISD(T)/6-311+G(3DF) energy (Hartrees)	T_e(eV)	R(1-2)(Å)	R(1-3)(Å)	α	Frequencies (cm^{-1})/ΔQ(Å $amu^{1/2}$)[b]
Si_4^-	$^2B_{2g}(D_{2h})$	−1156.209 09	−2.06	2.303	2.352	90.0°	361(a_g), 485(a_g)
Si_4	$^1A_g(D_{2h})$	−1156.133 24	0.0	2.312	2.413	90.0°	332(a_g)/0.19, 463(a_g)/0.15
	$^3B_{3u}(D_{2h})$	−1156.101 85	0.85	2.265	2.544	90.0°	330(a_g)/1.07, 480(a_g)/0.04[c]
	$^3B_g(C_{2h})$	−1156.078 06	1.50	2.285;2.383	2.219	87.3°	148(a_g)/0.38, 372(a_g)/1.36, 529(a_g)/0.36
	$^3B_{1g}(D_{2h})$	−1156.070 41	1.71	2.352	2.280	90.0°	353(a_g)/0.64, 491(a_g)/0.08
	$^3B_{1u}(D_{2h})$	−1156.060 20	1.99	2.378	2.443	90.0°	329(a_g)/0.22, 440(a_g)/0.52

[a]MP2 frequencies are scaled by 0.95. (Ref. 6) Geometries, frequencies, and energies from Ref. 17.
[b]Only totally symmetric modes (a_g) are listed.
[c]QCISD/6-31G* frequencies from Ref. 27; normal coordinate displacements based on QCISD/6-31G* geometries and force constants.

TABLE III. MP2/6-31G* optimized geometries, frequencies, and normal coordinate displacements[a] for Si_5.

	States	T_e(eV)	R(1-2)(Å)	R(1-3)(Å)	R(1-4)(Å)	R(3-4)(Å)	Angle(4-3-5)	Frequencies (cm^{-1})/ΔQ(Å $amu^{1/2}$)[b]
Si_5^-	$^2A_2''(D_{3h})$	−2.14	3.468	2.326	2.326	2.685	60.0°	473(a_1'), 309(a_1')
Si_5	$^1A_1'(D_{3h})$	0	3.057	2.296	2.296	2.967	60.0°	476(a_1')/0.21, 247(a_1')/2.12
	$^3B_1(C_{2v})$	0.5	3.575	2.294	2.361	2.483	69.8°	494(a_1)/0.70, 373(a_1)/0.48, 364(a_2)/0.71, 320(a_1)/0.29, 159(a_1)/0.99

[a]MP2 frequencies are scaled by 0.95 (Ref. 6).
[b]Only totally symmetric modes (a_1') are listed.

TABLE IV. MP2/6-31G* optimized geometries, frequencies,[a] and normal coordinate displacements for Si_6.

	States	T_e(eV)	R(1-2)(Å)	R(1-3)(Å)	R(3-4)(Å)	Frequencies (cm^{-1})/ΔQ(Å $amu^{1/2}$)[b]
Si_6^-	$^2A_{2u}(D_{4h})$	−1.45	3.114	2.397	2.577	444(a_{1g}), 306(a_{1g})
Si_6	$^1A_{1g}(D_{4h})$	0	2.694	2.356	2.734	447(a_{1g})/0.49, 298(a_{1g})/1.90
	$^3E_g(D_{4h})$	1.26	3.282	2.413	2.501	
	$^3B_{lu}(D_{4h})$	3.44	3.156	2.441	2.632	

[a]MP2 frequencies are scaled by 0.95. Geometries and frequencies are the same as in Ref. 6.
[b]Only totally symmetric modes (a_{1g}) are listed.

TABLE V. MP2/6-31G* optimized geometries, frequencies,[a] and normal coordinate displacements for Si_7.

	States	T_e(eV)	R(1-2)(Å)	R(1-3)(Å)	R(3-4)(Å)	Frequencies (cm^{-1})/ΔQ(Å $amu^{1/2}$)[b]
Si_7^-	$^2A_2''(D_{5h})$	−1.25	2.837	2.507	2.431	407(a_1'), 295(a_1')
Si_7	$^1A_1'(D_{5h})$	0	2.512	2.457	2.483	440(a_1')/0.67, 352(a_1')/1.15

[a]MP2 frequencies are scaled by 0.95. Geometries and frequencies are the same as in Ref. 6.
[b]Only totally symmetric modes (a_1') are listed.

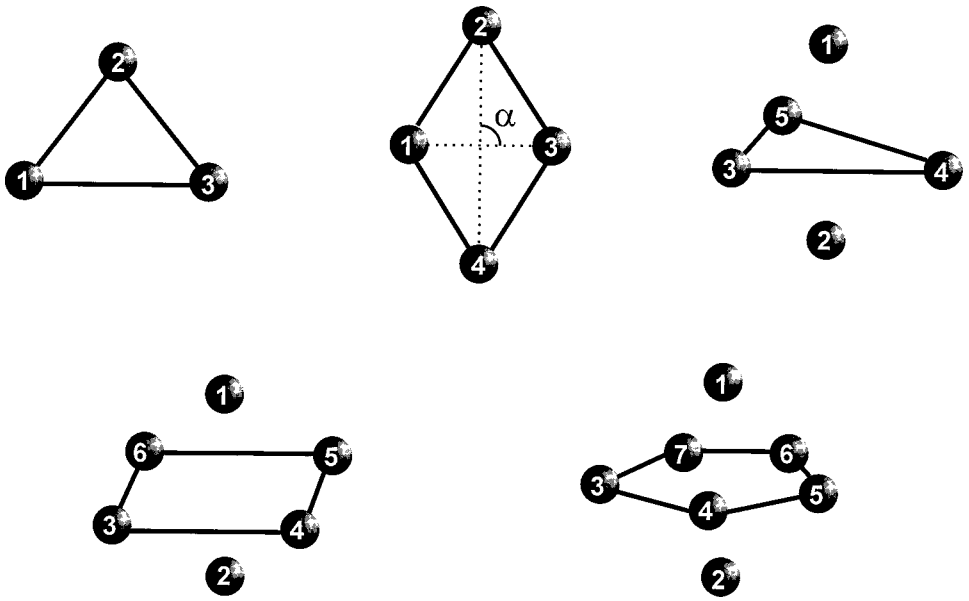

FIG. 10. Geometries of the silicon clusters studied in the current work.

$=0.476$ eV with an average spacing of 323 ± 20 cm^{-1}. Band *B* at low eKE is the most intense transition. It corresponds to another low-lying electronic state and only the onset of this band was observed at 355 nm. Band *X* is isotropic with $\beta=0$. Bands *A* and *B* have negative β parameters of -0.3 and -0.2, respectively.

The Si_7^- spectra at 416 and 355 nm in Figs. 8 and 9, respectively, show evidence for two bands, labeled *X* and *A*. Band *X* shows a progression of ten peaks spaced by 385 ±20 cm^{-1}; this progression is slightly better resolved at 416 nm. At the higher wavelength, the onset of band *X* occurs at eKE$\cong$1.0 eV. At 355 nm band *A* dominates the spectrum at low electron kinetic energies, with a β parameter of -0.3. As shown in the top panel of Fig. 9, β for band *X* varies from -0.5 to 0.5 as the electron energy decreases.

Assignment of the electronic and vibrational features in the experimental spectra is greatly facilitated by *ab initio* calculations of the geometries, vibrational frequencies, force constants, and state energies. From these, one obtains normal coordinate displacements for photodetachment to each neutral state. The displacements are calculated within the parallel mode approximation, in which the force constants for the neutral state are assumed for both the anion and neutral. One can then perform Franck–Condon simulations of the spectrum based on the *ab initio* calculations and compare with experiment.

Tables I and II summarize the *ab initio* results for Si_3^-/Si_3 and Si_4^-/Si_4. Most of these are from published and unpublished calculations at the MP2 and QCISD(T) levels performed by Rohlfing;[17,27] the MP2 frequencies for the $^3B_{3u}$, $^3B_{1g}$, and $^3B_{1u}$ states of Si_4 are from our calculations using GAUSSIAN 92,[28] as are the normal coordinate displacements for all the Si_4 states in Table II. In these tables, geometries were optimized and frequencies and force constants are calculated at the QCISD(T)/6-31G* level for Si_3^-/Si_3 and at the MP2/6-31G* level for Si_4^-/Si_4. Electronic state energies are then calculated at the QCISD(T) level using the larger 6-311+G(3DF) basis. We also calculated geometries, frequencies, and force constants for various electronic states of Si_5, Si_6, and Si_7 at the MP2/6-31G* level of theory; these along with previous calculations by Honea *et al.*[6] are summarized in Tables III–V. Note that low-lying, open shell singlet states are expected for many of these clusters but cannot be calculated with the methods used here. The geometries of the silicon clusters used in these tables are shown in Fig. 10.

IV. ANALYSIS AND DISCUSSION

A. General

In this section, the photoelectron spectra are analyzed and assignments of the various bands made, when possible. The assignments are facilitated by comparison with previous *ab initio* studies as well as calculations performed as part of this investigation. Spectral simulations of the vibrational profiles based on the Franck–Condon approximation are also very useful in assigning the bands, as are the photoelectron angular distributions. In the case of Si_3^- and Si_4^- where there has already been considerable discussion of the anions and the ground and lowest excited states of the neutrals, the discussion below focuses more on the higher-lying states that are better characterized experimentally in the spectra presented here. The larger clusters have received less attention so all aspects of their photoelectron spectra are considered below.

B. Si_3^-

Several *ab initio* calculations have been performed on Si_3^- and the low-lying states of Si_3.[8–11,16–19,29,30] The ground state of the anion is predicted to have C_{2v} symmetry with the valence electron configuration $\cdots(10a_1)^2(3b_1)^2(7b_2)^2$

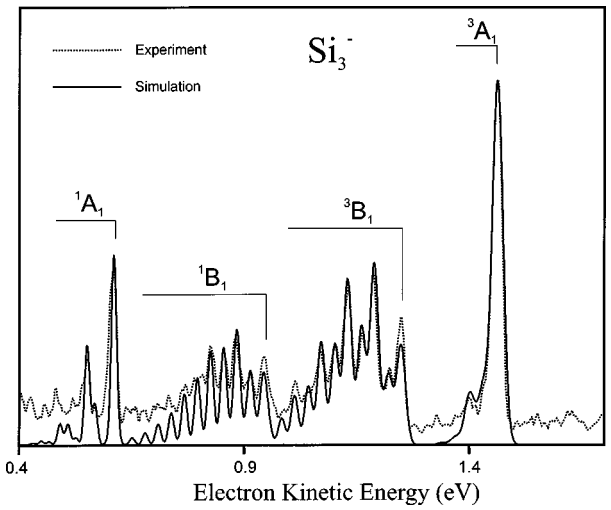

FIG. 11. Franck–Condon simulation of the Si_3^- spectrum. Parameters given in Table VI.

$(11a_1)^1$, yielding a $^2A_1$ state. The neutral $^1A_1$ ground state is formed by photodetaching an electron from the highest occupied molecular orbital (HOMO), the $11a_1$ orbital, of the anion. The low-lying electronic states accessible via anion photoelectron spectroscopy are the singlet and triplet pairs of the B_2, B_1, and A_1 states, corresponding to removal of an electron from the $7b_2$, $3b_1$, and $10a_1$ orbitals, respectively. The $^3B_2$ state collapses to a D_{3h} $^3A_2'$ state, 0.02 eV above the ground state. *Ab initio* results at the QCISD(T) level[17,27] for the anion and neutral ground states and several triplet states of Si_3 are listed in Table I.

In our previous photoelectron spectrum of Si_3^-, five bands (*C* and *D* in Fig. 3 were labeled as a single band *C*) were observed at 266 nm.[2]. Band *X* was also investigated by ZEKE spectroscopy of Si_3^-.[4] Based on the experimental and theoretical results, band *X* was assigned to overlapped transitions to the $^1A_1$ ground state and the low-lying $^3A_2'$ state. Rohlfing and Raghavachari assigned bands *A*, *B*, *C*, and *D* to the $^1B_2$, $^3A_1$, $^3B_1$, and $^1B_1$ states, respectively, based on their calculations at the QCISD(T) level for the triplet states and at the single excitation CI level (CIS) for the open shell singlets.[17] Since band *C* is now resolved to be two distinct bands (*C* and *D* in Fig. 3) some new assignments are required.

The assignments of bands *X*, *A*, and *B* are unchanged. To aid in assigning the higher energy bands, we obtained the normal coordinate displacements from the anion ground state to the neutral states, using the geometries and force constants from the QCISD(T)/6-31G* calculations for the excited triplet states.[17] These displacements are obtained within the parallel mode approximation in which the force constants for the relevant neutral electronic state are used for both the neutral and the anion. Given these displacements, one can simulate the photoelectron spectrum within the Franck-Condon approximation. For some bands, the normal coordinate displacements were adjusted to obtain a better fit to the experimental spectrum. Simulations of bands *B*–*E* are shown in Fig. 11 superimposed on the experimental data; the parameters used in the simulations are listed in Table VI.

The appearance of band *B* indicates that the molecular geometries of the anion and neutral electronic states are very similar, consistent with the *ab initio* results. To simulate the spectrum of band *B* in Fig. 11, we used symmetric stretch and bend frequencies $\nu_1=500\ \mathrm{cm}^{-1}$ and $\nu_2=250\ \mathrm{cm}^{-1}$, respectively, and normal-mode displacements $\Delta Q_1=0.13$ Å $\mathrm{amu}^{1/2}$ and $\Delta Q_2=0.19$ Å $\mathrm{amu}^{1/2}$. These values agree reasonably well with the QCISD(T) values of $\nu_1=523\ \mathrm{cm}^{-1}$ and $\Delta Q_1=0.09$ Å $\mathrm{amu}^{1/2}$, and $\nu_2=325\ \mathrm{cm}^{-1}$ and $\Delta Q_2=0.05$ Å $\mathrm{amu}^{1/2}$. We also obtain a new term energy of $T_0(^3A_1)=0.90\pm0.02$ eV from our simulation, in good agreement with the QCISD(T) value of 0.92 eV.[17]

Bands *C* and *D* have approximately equal β parameters of 0.2 and 0, respectively. The similarity of the vibrational

TABLE VI. Term energies, frequencies, and normal coordinate displacements used in the simulations.

			Frequencies (cm^{-1})/ΔQ(Å $\mathrm{amu}^{1/2}$)			
	States	T_0(eV)[a]	ν_1	ΔQ_1	$\nu 2$	ΔQ_2
Si_3	$^3A_1(C_{2v})$	0.90	500	0.13	250	0.19
EA=2.29±0.02 eV	$^3B_1(C_{2v})$	1.12	480, $x_1=0.5$[b]	0.46	225	0.40
	$^1B_1(C_{2v})$	1.43	475, $x_1=1.0$	0.40	235	0.50
	$^1A_1(C_{2v})$	1.76	480	0.23	340	0.20
Si_4	$^3B_{3u}(D_{2h})$	0.85	450	0.18	308	1.14
EA=2.13±0.01 eV	$^1B_{3u}(D_{2h})$	1.34	490	0.05	290	1.15
	$^3B_{1g}(D_{2h})$	1.71	517	0.15	355	0.72
	$^3B_{1u}(D_{2h})$	1.93	448	0.65	346	0.22
Si_5	$^1A_1'(D_{3h})$	0.0	501	0.21	233	2.12
EA=2.59±0.02 eV	$^3B_1(C_{2v})$	1.16±0.05				
Si_7	$^1A_1'(D_{5h})$	0.0	463	0.67	385	1.15
EA=1.85±0.02 eV	$^1A_1(C_{3v})$	1.14±0.05				

[a]The error bars are ±0.02 eV, except noticed.
[b]x_1 is the anharmonicity used in the simulations.

progressions shows that the two neutral states have similar geometries and frequencies. These two observations indicate that the neutral states probably have the same molecular orbital configuration. We therefore assign bands *C* and *D* to the $^3B_1$ and $^1B_1$ states, respectively. This yields a term value for the $^3B_1$ state, 1.12 ± 0.02 eV, which is in excellent agreement with the previously calculated term value of 1.12 eV.[17] The resulting singlet-triplet splitting of 0.31 ± 0.01 eV based on the apparent band origins is somewhat lower than the calculated value of 0.41 eV by Sabin *et al.*,[10] but is clearly in the right range. The QCISD(T)/6-31G* calculation[17] for the $^3B_1$ state gives $\Delta Q_1=0.41$ Å amu$^{1/2}$ and $\Delta Q_2=0.38$ Å amu$^{1/2}$. Similar normal coordinate displacements are expected for the $^1B_1$ state, so both the symmetric stretch (ν_1) and bend (ν_2) modes should be active in the $^3B_1$ and $^1B_1$ states. The Franck–Condon simulations of these two transitions are shown in Fig. 11. The parameters used in the simulations, listed in Table VI, show that the vibrational frequencies and normal coordinate displacements for the two neutral states are quite similar to one another and in good agreement with the calculated values for the $^3B_1$ state in Table I.

Band *E* was originally assigned to the $^1B_1$ state. Given our new assignment of band *D* to this state, we assign band *E* to the open-shell $^1A_1$ state, the singlet counterpart of the $^3A_1$ state (band *B*), corresponding to removal of an electron from the $10a_1$ orbital. Our assignment is supported by the polarization results, which show bands *B* and *E* have similar β parameters, and by the similar vibrational progressions in the two bands. Since the ground state is also a $^1A_1$ state, we were not able to perform an SCF calculation on this higher energy $^1A_1$ state. The simulation shown in Fig. 11 was obtained using the parameters $\nu_1=480$ cm^{-1}, $\Delta Q_1=0.23$ Å amu$^{1/2}$, and $\nu_2=340$ cm^{-1}, $\Delta Q_2=0.20$ Å amu$^{1/2}$. These frequencies and normal coordinate displacements are similar to those for photodetachment to the $^3A_1$ state, supporting our singlet-triplet pair assignment.

C. Si_4^-

Ab initio calculations show that the ground state of Si_4^- is a rhombus with D_{2h} symmetry. The valence orbital configuration is $\cdots(b_{3u})^2(a_g)^2(b_{1u})^2(b_{2g})^1$ yielding a $^2B_{2g}$ electronic state.[17] Photodetachment from the b_{2g} HOMO yields the ^1A_g neutral ground state which is also a rhombus.[13] Removal of electrons from other orbitals yields low-lying excited states that are accessible via anion photoelectron spectroscopy. From the *ab initio* calculations[17,27] in Table II, the low-lying triplet states in order of increasing energy are the $^3B_{3u}$, ^3B_g, $^3B_{1g}$, and $^3B_{1u}$ states; all have D_{2h} symmetry except the ^3B_g state with C_{2h} symmetry which results from slight geometric distortion of a $^3B_{2g}(D_{2h})$ state. Calculated energies, geometries, frequencies, and normal coordinate displacements are also shown in Table II. Each triplet excited state has a corresponding open-shell singlet state which has not been calculated here. A simulation of the Si_4^- photoelectron spectrum resulting from photodetachment to several of these excited states is shown in Fig. 12. The simulation parameters are shown in Table VI.

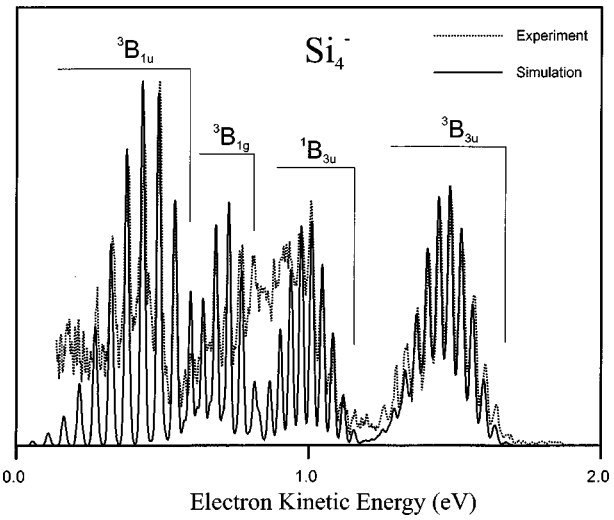

FIG. 12. Franck–Condon simulation of the Si_4^- spectrum. Parameters given in Table VI.

The ground state, band *X*, is best seen in the 355 nm photoelectron spectrum (Fig. 2). The electron affinity was measured to be 2.15 eV from our earlier photoelectron spectrum.[2] The new spectrum is slightly better calibrated through comparison with the ZEKE spectrum of Si_4^-.[3] The spectrum in Fig. 2 shows a progression of three peaks spaced by 380 ± 20 cm^{-1} in band *X*, corresponding to photodetachment to the ^1A_g ground state. The band is dominated by the vibrational origin at eKE=1.365 eV, yielding a new Si_4 electron affinity of 2.13 ± 0.01 eV.

Band *A* was studied by ZEKE spectroscopy[3] in some detail, and a comparison with theory confirmed that this band corresponds to the transition to the $^3B_{3u}$ state, resulting from photodetachment from the b_{1u} orbital.[17] Several vibrational frequencies were obtained. The $^3B_{3u}$ state has two totally symmetric vibrational modes, the ν_1 overall stretch and ν_2 symmetric distortion modes. In addition there are three asymmetric stretching modes (ν_3, ν_4, and ν_5), and a bending mode of b_{3u} symmetry (ν_6). The ν_2 mode has the largest displacement upon photodetachment, resulting in the main progression of 310 ± 20 cm^{-1} in the 266 nm spectrum. This is in good agreement with the ZEKE spectrum which yielded a frequency of $\nu_2=312$ cm^{-1}.

Band *B* appeared as a very short progression in the ZEKE spectrum and was assigned to the $^1B_{3u}$ state. In Fig. 4, band *B* consists of a longer progression of peaks spaced by 290 ± 20 cm^{-1}, in good agreement with the ZEKE value of 300 cm^{-1} and close to the ν_2 frequency in the $^3B_{3u}$ state. Bands *A* and *B* exhibit similar peak spacings and intensity profiles. Moreover, the anisotropy parameters are similar: $\beta=0.3$ for band *B* and 0.5 for band *A*. These observations support the previous assignment of band *B* to the $^1B_{3u}$ state, which has the same molecular orbital configuration as the $^3B_{3u}$ state. Band *B* can be simulated using almost the same normal coordinate displacements as band *A*. The simulation

of band *B* shown in Fig. 12 yields a term energy of 1.34 ± 0.02 eV for the $^1B_{3u}$ state, and a $^1B_{3u}-{}^3B_{3u}$ singlet-triplet splitting of 0.49 ± 0.02 eV.

Band *C* does not show a regular progression, and it has the most positive β parameter (0.8) of all the bands. The QCISD(T) energy calculations predict the term value of the ^3B_g state to be 1.50 eV. The corresponding electron kinetic energy of 1.04 eV is just where band *C* is found. Moreover, the ^3B_g state is a lower symmetry, Jahn–Teller distorted state, so an additional low-frequency bending vibration ($156\ \mathrm{cm}^{-1}$ in Table II) is totally symmetric. This mode should also be active ($\Delta Q_3=0.38$ Å amu$^{1/2}$ in Table II) due to the symmetry change upon photodetachment along with the other two modes. One therefore expects a higher density of vibrational transitions which, given the resolution of our spectrometer, might well result in the absence of a clear vibrational progression. We therefore assign band *C* to the ^3B_g state.

Band *D* shows a single progression of $355\pm 20\ \mathrm{cm}^{-1}$. From Table II, the $^3B_{1g}$ state of Si_4 is predicted to lie in this energy range, and the calculated normal coordinate displacements for photodetachment to this state are significant only for a single vibrational mode with frequency $353\ \mathrm{cm}^{-1}$. Band *D* is therefore assigned to the $^3B_{1g}$ state. The simulation of photodetachment to the $^3B_{1g}$ state is shown in Fig. 12. Due to overlap with band *C*, the band origin is difficult to locate. Figure 12 shows the best fit to the experimental vibrational profile. The resulting term energy of $T_0(^3B_{1g})=1.71\pm 0.02$ eV is in excellent agreement with the calculated value in Table II, and the normal coordinate displacements used in the simulations are in reasonable agreement with the calculated displacements, further supporting this assignment.

Band *E* stands alone with well-resolved vibrational structure. It lies about 2 eV above the ground state and the peak spacing is $451\pm 20\ \mathrm{cm}^{-1}$. The *ab initio* calculation predicts a term energy of 1.99 eV for the $^3B_{1u}$ state, and a large displacement of $\Delta Q_1=0.52$ Å amu$^{1/2}$ along the ν_1 mode for which the frequency is $440\ \mathrm{cm}^{-1}$. Although the calculated $\Delta Q_2=0.22$ Å amu$^{1/2}$, the resulting Franck–Condon profile in this mode is much shorter than for the ν_1 mode because of the smaller frequency of $346\ \mathrm{cm}^{-1}$. We therefore assign band *E* to the $^3B_{1u}$ state, which is the only state in Table II for which ΔQ is largest for the ν_1 mode. A term energy of $T_0(^3B_{1u})=1.93\pm 0.02$ eV is obtained from the simulation shown in Fig. 12, slightly lower than the *ab initio* term value. Agreement between the simulated and *ab initio* normal coordinate displacements is satisfactory.

One might argue that either band *D* or *E* is due to the $^1B_{2g}$ state, the singlet counterpart of the ^3B_g state responsible for band *C*. Although the vibrational profile of band *C* is quite different from the other two, the $^1B_{2g}$ state is not expected to undergo geometric distortion from C_{2v} symmetry,[17] so this alone does not rule out an alternate assignment. However, the anisotropy parameter $\beta=0.8$ for band *C*, while $\beta=0$ and -0.1 for bands *D* and *E*, respectively. Thus it is unlikely that either band is from the $^1B_{2g}$ state. The question remains as to the location of the $^1B_{2g}$ state. Rohlfing predicts a singlet-triplet splitting of only 0.17 eV for the $^1B_{2g}$ and ^3B_g states. Either this value is too low, or the transition to the $^1B_{2g}$ state overlaps with band *C*. The latter is certainly possible given the broad, unstructured appearance of band *C*. This issue can be addressed by higher level *ab initio* calculations.

D. Si_5^-

Little is known about the ground and excited states of Si_5 from previous experimental studies. The concentration of Si_5 was presumably too low to be observed in earlier matrix spectroscopy studies.[6,7] The photoelectron spectra of Si_5^- obtained by Cheshnovsky *et al.*[1] did not have sufficient resolution to map out any vibrational structure.

More information is available from the *ab initio* calculations by Raghavachari and Rohlfing, which predicted that Si_5 and Si_5^- have compressed trigonal bipyrimidal ground states with D_{3h} symmetry.[9,15] The molecular orbital configuration for Si_5^- is $\cdots(e'')^4(a_1')^2(e')^4(a_2'')^1$, yielding a $^2A_2''$ ground state. Removal of an electron from the HOMO leaves a closed-shell neutral $^1A_1'$ ground state. Si_5 was also predicted to have a low-lying $^3B_1$ triplet state with a Jahn–Teller distorted C_{2v} structure. The molecular orbital configuration of this state is $\cdots(a_1)^2(a_2)^2(b_1)^2(b_2)^2(b_1)^1(a_1)^1$ which correlates with the $\cdots(e'')^4(a_1')^2(e')^3(a_2'')^1)$ state of the trigonal bipyramid. The $^3B_1$ state is accessible by removal of an electron from the e' orbital in the anion. Calculations at the MP4/6-31G* level indicate that the $^3B_1$ state lies about 0.5 eV above the ground state.[15] *ab initio* results for Si_5^- and Si_5 are summarized in Table III.

In the Si_5^- spectrum taken at 355 nm (Fig. 5), band *X* consists of an extended progression with a peak spacing of $233\pm 10\ \mathrm{cm}^{-1}$ beginning around eKE=0.75 eV. This long progression indicates a large geometry change between the anion and the neutral electronic ground states. The $^1A_1'$ ground state is formed by photodetaching an electron from the a_2'' orbital which is antibonding between the two apex atoms. The *ab initio* calculations indicate that photodetachment to the $^1A_1'$ state results in a significant reduction of the distance between the apical atoms, leading to a large displacement along the totally symmetric ν_2 normal coordinate mode. The observed peak spacing is in good agreement with our MP2/6-31G* value of $\nu_2=247\ \mathrm{cm}^{-1}$ shown in Table III.

The anion, neutral geometries, and force constants from our MP2/6-31G* calculations have been applied to obtain the normal coordinate change between the anion and neutral. The Franck–Condon simulation of band *X* is shown in Fig. 13. The experimental ν_2 frequency was used, but the other parameters were taken directly from the MP2/6-31G* calculation: $\Delta Q_1=0.21$ Å amu$^{1/2}$, $\Delta Q_2=2.12$ Å amu$^{1/2}$, and $\nu_1=501\ \mathrm{cm}^{-1}$. The extraordinarily large normal coordinate displacement for ΔQ_2 results in poor overlap with the vibrational origin; this transition has no intensity in the simulated spectrum. To obtain the best fit, we chose the vibrational origin at 0.935 eV electron energy, yielding an electron affinity of 2.59 ± 0.02 eV for Si_6. Although one could obtain a satisfactory fit assuming the vibrational origin shifted by a

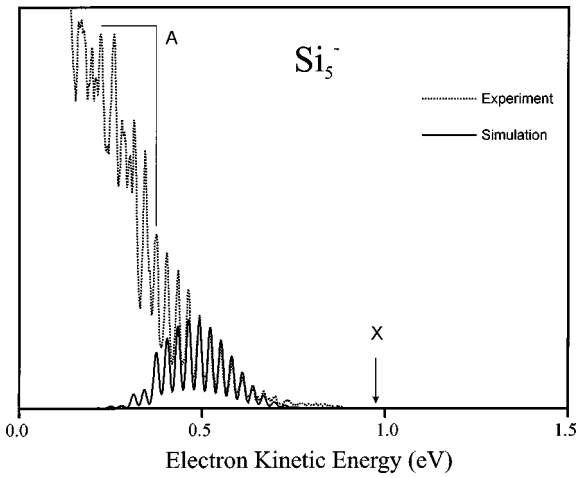

FIG. 13. Franck–Condon simulation of the Si_5^- spectrum. Parameters given in Table VI.

vibrational quantum in either direction, this required using normal coordinate displacements that differed more from the *ab initio* values. The adiabatic electron affinity from our assignment is 0.5 eV less than the vertical detachment energy of 3.10 eV calculated by Adamowicz.[31] This discrepancy is due at least in part to the large geometry change between the anion and neutral ground state. Raghavachari and Rohlfing[16] reported an adiabatic electron affinity of 2.26 eV at the QCISD(T)/6-31+G* level, in reasonable agreement with our experimental value.

The $^3B_1$ state excited state is a Jahn–Teller distorted C_{2v} state with four totally symmetric vibrational modes. One therefore expects a congested photoelectron spectrum to result from photodetachment to this state. The irregular vibrational structure of band *A* therefore suggests that we assign it as the transition to the $^3B_1$ state. From the spectrum at $\theta=0°$ in which the ground state has little intensity, we estimate the $^3B_1$ state origin to be at eKE$=0.36\pm0.05$ eV, 0.58 eV above the $^1A_1'$ ground state. This is in agreement with the calculated term value of 0.5 eV, further supporting our assignment.

Besides the *X* and *A* bands, a new band *B* shows up at low eKE in the 299 nm spectrum (Fig. 6). We estimate the origin of this band to occur at eKE$=0.39$ eV, yielding a term energy of 1.16 ± 0.05 eV for this neutral excited state.

E. Si_6^-

Ab initio calculations predict Si_6^- to have a $^2A_{2u}$ ground state with D_{4h} symmetry, corresponding to a tetragonal bipyramidal structure, with valence orbital configuration $\cdots(e_g)^4(a_{1g})^2(b_{2g})^2(e_u)^4(a_{2u})^1$.[16] Calculations also predict that neutral Si_6 has three nearly isoenergetic structures: a tetragonal bipyramid ($^1A_{1g}$,D_{4h}) and two in which this structure is distorted ($^1A_1$,C_{2v}). The $^1A_{1g}$ state corresponds to the removal of an electron from the a_{2u} HOMO. At the HF/6-31G* level, Raghavachari found the two C_{2v} structures are separated by 0.04 eV while the D_{4h} structure is about 0.4 eV higher in energy.[9] Fournier *et al.* reported similar results using density functional theory,[19] with the three structures lying within 0.2 eV of one another. At the MP2/6-31G* level, the $^1A_{1g}$ state with D_{4h} symmetry is preferred. The assignment of this structure as the ground state is consistent with the experimental vibrational frequencies from matrix Raman spectroscopy.[6] *Ab initio* results for the ground and excited states at the MP2/6-31G* level are summarized in Table IV.

In the 355 nm photoelectron spectrum, Fig. 7, the transition to the Si_6 ground state (band *X*) appears as a weak, unstructured band. For a D_{4h} tetragonal bipyramidal molecule, there are two totally symmetric modes ν_1 and ν_2. A Franck–Condon simulation using the frequencies and normal coordinate displacements in Table IV for photodetachment to the $^1A_{1g}$ state shows extended progressions in both modes, and this along with incomplete vibrational cooling may explain the absence of structure in band *X*. We note that this simulation (not shown) is considerably broader than the experimental band, indicating that the calculated normal coordinate displacements and/or vibrational frequencies need to be adjusted.

In contrast to band *X*, band *A* in Fig. 7 shows a progression of 323 ± 20 cm^{-1} between 0.25 and 0.50 eV. The presence of a single progression indicates that the neutral is at least as symmetric as the anion; if the anion has D_{4h} symmetry, band *A* should correspond to the transition to a state with D_{4h} or O_h symmetry. Although a low-lying triplet state with O_h symmetry was investigated in the calculation by Fournier *et al.*, it was predicted to have two imaginary frequencies.[19] We performed *ab initio* calculations on two low-lying states restricted to D_{4h} symmetry. At the MP2/6-31G* level, a ^3E_g state was found to lie 1.26 eV above the ground state, corresponding to the removal of an e_u electron from the anion $^2A_{2u}$ state. However, one imaginary frequency was also found at the HF/6-31G* level. Photodetaching a b_{2g} electron from the anion ground state results in a $^3B_{1u}$ state which is 3.44 eV less stable than the neutral $^1A_{1g}$ ground state. Neither state appears to be a likely candidate for band *A*. Alternatively, if the anion ground state had C_{2v} symmetry, then band *A* could be explained as a transition to the low-lying C_{2v} structures of Si_6 predicted by Raghavachari.[9] In any case, further theoretical work on the low-lying states of both Si_6 and Si_6^- appears needed to explain this band and the intense, unstructured band *B* at lower eKE.

F. Si_7^-

Si_7^- is predicted to have a pentagonal bipyramidal D_{5h} ground-state geometry.[15] The valence electron configuration is $\cdots(e_1'')^4(a_1)^2(e_1')^4(e_2')^4(a_2'')^1$, resulting in a $^2A_2''$ state. Photodetaching an electron from the HOMO orbital yields the $^1A_1'$ ground state of the neutral species, which also has D_{5h} symmetry. As the a_2'' orbital is antibonding between the apex atoms, detachment to the $^1A_1'$ state results in a more compact structure along the apex, just as for Si_5^-. The $^1A_1'$ state has two totally symmetric stretch modes (ν_1 and ν_2). The optimized geometries, frequencies, and resulting normal-mode displacements at the MP2/6-31G* level are

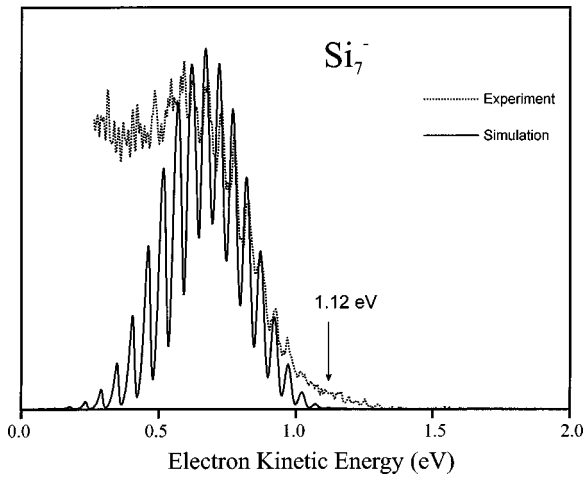

FIG. 14. Franck–Condon simulation of the Si_7^- spectrum. Parameters given in Table VI.

shown in Table V. Raghavachari and Rohlfing studied two other isomers, a tricapped trigonal pyramid and a capped octahedral structure, both of C_{3v} symmetry. They were found to be 0.95 and 2.08 eV less stable than the $^1A_1'$ state at the MP4/6-31G* level, respectively.[15]

In the Si_7^- photoelectron spectrum at 416 nm (Fig. 8), band *X* shows a resolved vibrational progression with a peak spacing of $385\pm20\ cm^{-1}$. Comparison to Table V shows that this frequency lies between the calculated values for the two totally symmetric modes of the $^1A_1'$ state. However, the experimental value is closer to the calculated ν_2 frequency $(352\ cm^{-1})$, and the calculated normal coordinate displacement is considerably larger for the ν_2 mode. We therefore assign the observed progression to this mode. Figure 14 shows a simulated spectrum in which only the ν_2 frequency is changed from the *ab initio* values. Note that although the ν_2 progression dominates, the ν_1 mode is also active, resulting in only partial resolution of the ν_2 progression in the simulation and, presumably, the experiment. The vibrational origin at eKE=1.12 eV yields an electron affinity of 1.85 $\pm$0.02 eV for Si_7. While acceptable simulations at different origins can be achieved by changing the normal-mode displacements, the best results are obtained with the values reported here. Raghavachari and Rohlfing reported an electron affinity of 1.7 eV at the MP2/6-31G* level.[16]

Recently, Eberhardt reported the vibrationally resolved photoelectron spectrum of annealed Si_7^- at a photon energy of 2.897 eV photon energy.[5] They measured a frequency of $380\pm20\ cm^{-1}$ for Si_7. This is very close to our value, but both gas phase values are slightly less than the vibrational frequency of $435\ cm^{-1}$ seen in the matrix Raman experiment.[6] This discrepancy may be due to matrix effects.

The photoelectron spectrum at 355 nm (Fig. 9) shows band *X* in its entirety and the onset of a second band labeled band *A* at low eKE. The origin of band *A* was estimated as the intercept resulting from an extrapolation of the linear portion of this band in the photoelectron spectrum to the energy axis. The best estimate of 0.50 eV electron energy corresponds to a term energy of 1.14$\pm$0.05 eV. Raghavachari and Rohlfing found a C_{3v} tricapped tetrahedron isomer of a $^1A_1$ state which lies 0.95 eV above the $^1A_1'$ ground state at the MP4/6-31G* level.[15] We therefore assign band *A* to this excited state.

The anisotropy parameter β for band *X* varies significantly with electron energy, as shown in the top panel of Fig. 9. This could signify that transitions to two neutral electronic states with different polarization dependence contribute to band *X*. However, this would require an open-shell excited state of Si_7 with nearly the same energy as the $^1A_1'$ state. The low electron affinity of Si_7 suggests that the $^1A_1'$ state is particularly stable, so this is an unlikely scenario. Moreover, no variation of β occurs in the photoelectron spectrum at 416 nm in Fig. 8. An alternative explanation is that there is an excited electronic state of Si_7^- near 355 nm, and that autodetachment from this state contributes to the photoelectron spectrum along with direct detachment.

V. CONCLUSIONS

The anion photoelectron spectra presented here provide new information on the ground and low-lying electronic states of silicon clusters. Several new assignments of the excited state bands are based on the vibrational structure that is resolved in many of these spectra, the angular distribution of the photoelectrons, and comparison with *ab initio* calculations. For Si_3 and Si_4, all excited states accessible via photodetachment with $T_0<2.5$ eV have been assigned. Vibrational frequencies are obtained for the ground states of Si_5 and Si_7. In both cases, an extended progression is observed for a single, totally symmetric vibrational mode, indicating a substantial geometry change but no change in symmetry upon photodetachment. This progression corresponds to excitation in the ν_2 symmetric distortion mode of the neutral cluster, resulting from a considerable reduction in the spacing between the apical Si atoms upon photodetachment. In the Si_6^- spectra, vibrational structure was resolved for a low-lying excited state, the identity of which still needs to be determined.

ACKNOWLEDGMENTS

This work is supported by the National Science Foundation under Grant No. DMR-9521805. Support from the National Energy Research Scientific Computing Center (NERSC) is gratefully acknowledged. We thank C. M. Rohlfing for communicating results from calculations and for helpful discussions and comments regarding the manuscript.

[1] O. Cheshnovsky, S. H. Yang, C. L. Pettiette, M. J. Craycraft, Y. Liu, and R. E. Smalley, Chem. Phys. Lett. **138**, 119 (1987).
[2] T. N. Kitsopoulos, C. J. Chick, A. Weaver, and D. M. Neumark, J. Chem. Phys. **93**, 6108 (1990).
[3] C. C. Arnold and D. M. Neumark, J. Chem. Phys. **99**, 3353 (1993).
[4] C. C. Arnold and D. M. Neumark, J. Chem. Phys. **100**, 1797 (1994).
[5] G. S. Ickingkonert, H. Handschuh, P. S. Bechthold, G. Gantefor, B. Kessler, and W. Eberhardt, Surf. Rev. and Lett. **3**, 483 (1996).
[6] E. C. Honea, A. Ogura, C. A. Murray, K. Raghavachari, W. O. Sprenger, M. F. Jarrold, and W. L. Brown, Nature (London) **366**, 42 (1993).
[7] S. Li, R. J. Vanzee, W. Weltner, and K. Raghavachari, Chem. Phys. Lett. **243**, 275 (1995).

[8] R. S. Grev and H. F. Schaefer, Chem. Phys. Lett. **119**, 111 (1985).
[9] K. Raghavachari, J. Chem. Phys. **84**, 5672 (1986).
[10] J. R. Sabin, J. Oddershede, G. H. F. Diercksen, and N. E. Gruner, J. Chem. Phys. **84**, 354 (1986).
[11] K. Balasubramanian, Chem. Phys. Lett. **125**, 400 (1986).
[12] K. Balasubramanian, Chem. Phys. Lett. **135**, 283 (1987).
[13] G. Pacchioni and J. Koutecky, J. Chem. Phys. **84**, 3301 (1986).
[14] P. Ballone, W. Andreoni, R. Car, and M. Parrinello, Phys. Rev. Lett. **60**, 271 (1988).
[15] K. Raghavachari and C. McMichael Rohlfing, J. Chem. Phys. **89**, 2219 (1988).
[16] K. Raghavachari and C. M. Rohlfing, J. Chem. Phys. **94**, 3670 (1991).
[17] C. M. Rohlfing and K. Raghavachari, J. Chem. Phys. **96**, 2114 (1992).
[18] D. A. Dixon and J. L. Gole, Chem. Phys. Lett. **188**, 560 (1992).
[19] R. Fournier, S. B. Sinnott, and A. E. Depristo, J. Chem. Phys. **97**, 4149 (1992).
[20] S. D. Li, R. L. Johnston, and J. N. Murrell, J. Chem. Soc. Faraday Trans. **88**, 1229 (1992).
[21] L. Adamowicz, Chem. Phys. Lett. **188**, 131 (1992).
[22] A. Rubio, J. A. Alonso, X. Blase, L. C. Balbas, and S. G. Louie, Phys. Rev. Lett. **77**, 247 (1996).
[23] R. B. Metz, A. Weaver, S. E. Bradforth, T. N. Kitsopoulos, and D. M. Neumark, J. Phys. Chem. **94**, 1377 (1990).
[24] C. Xu, G. R. Burton, T. R. Taylor, and D. M. Neumark, J. Chem. Phys. **107**, 3428 (1997).
[25] D. L. Osborn, D. J. Leahy, D. R. Cyr, and D. M. Neumark, J. Chem. Phys. **104**, 5026 (1996).
[26] J. Cooper and R. N. Zare, in *Lectures in Theoretical Physics* edited by S. Geltman, K. T. Mahanthappa, and W. E. Brittin (Gordon and Breach, New York, 1969), Vol. XI-C, pp. 317–337.
[27] C. Rohlfing (private communication).
[28] GAUSSIAN 92 , M. J. Frisch, G. W. Trucks, M. Head-Gordon, P. M. W. Gill, M. W. Wong, J. B. Foresman, B. G. Johnson, H. B. Schlegel, M. A. Robb, E. S. Replogle, R. Gomperts, J. L. Andres, K. Raghavachari, J. S. Binkley, C. Gonzalez, R. L. Martin, D. J. Fox, D. J. Defrees, J. Baker, J. J. P. Stewart, and J. A. Pople (Gaussian, Inc., Pittsburgh, PA, 1992).
[29] G. H. F. Diercksen, N. E. Grüner, J. Oddershede, and J. R. Sabin, Chem. Phys. Lett. **117**, 29 (1985).
[30] K. Raghavachari, J. Chem. Phys. **83**, 3520 (1985).
[31] L. Adamowicz, Chem. Phys. Lett. **180**, 466 (1991).